Crystallography Reports, Vol. 50, No. 1, 2005, pp. 20–26. From Kristallografiya, Vol. 50, No. 1, 2005, pp. 27–33.

DIFFRACTION AND SCATTERING OF IONIZING RADIATION

Indications of the Magnetic State in the Charge Distributions of MnO, CoO, and NiO. III: Antiferromagnetism of NiO[1]

J. -P. Vidal*, G. Vidal-Valat*, and K. Kurki-Suonio**

** Laboratoire d'Analyse Multipolaire des Répartitions de Charges Expérimentales, Université Montpellier 2, 34095 Montpellier Cedex 05, France*

e-mail: jpgvidal@univ-montp2.fr

*** Department of Physics, University of Helsinki, P.O. Box 64, FIN-00014, Finland*

Received July 2, 2002

Abstract—X-ray diffraction intensities were measured from antiferromagnetic NiO. The data were submitted to a nonparametric multipole analysis aimed at formulation of experimentally valid statements on the nature of charge distribution. Strong "bonding maxima" appear between the Ni⟨100⟩O nearest neighbors in the region of the oxygen atoms involving NiO coupling. An electronic cage structure is also observed. This is parallel to the observations on MnO and CoO but different in nature, being formed by separate cubic cages for the cations instead of the oxygen, and without a clear indication of an extended network buildup. © *2005 Pleiades Publishing, Inc.*

INTRODUCTION

This is the third part of an investigation aiming at finding characteristics of the different magnetic states of the first-row transition metal monoxides MnO, CoO, and NiO with help of a multipolar interpretation of their charge densities on the basis of accurate X-ray diffraction data. This paper reports the study of NiO at 298 K, where it is antiferromagnetic and weakly covalent.

The background of the investigation has been discussed in detail in the preceding papers concerning MnO and CoO [1, 2]. In addition, only in paper [3] was there any mention of the periodic Hartree–Fock method

[1] This article was submitted by the authors in English.

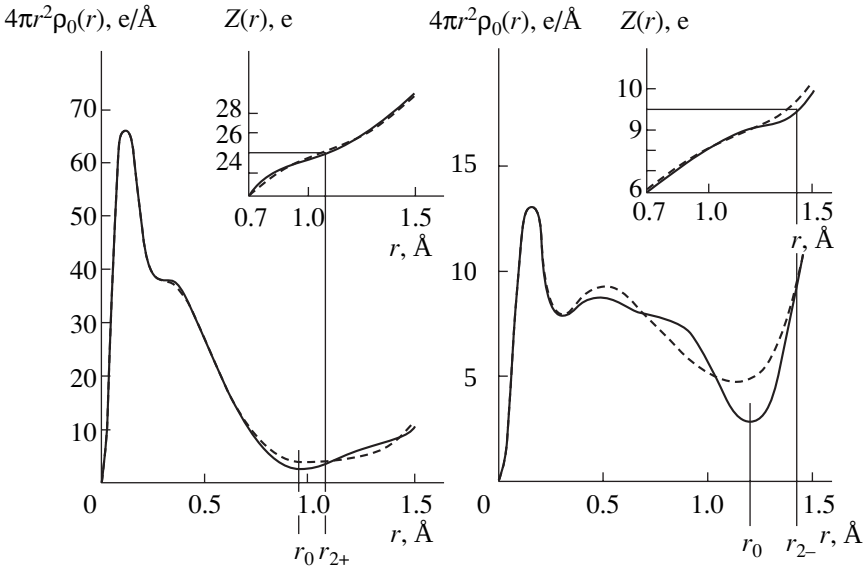

Fig. 1. Radial accumulation-of-charge densities $s_0(r)$ and electron counts $Z_0(r)$ around the ionic sites in the antiferromagnetic state of NiO at 298 K: experimental (solid lines), and reference model (dashed lines). The radii r_0 of "best separation," or minimum s_0, and the radii r_{2+} and r_{2-}, where the electron counts that correspond to double ionization of the ions are indicated for the experimental curves.

1063-7745/05/5001-0020$26.00 © 2005 Pleiades Publishing, Inc.

for calculation of electronic and magnetic properties of NiO. Description in terms of Mulliken charges yields, for example, values for net charges and bond populations. These parameters, tied by definition to the theoretical basis sets, are, however, not directly comparable with our results representing the integral properties of the experimental charge density or their deviations from the most simple charge-density model.

Preparation of the NiO sample and experimental procedures, as well as treatment of data, were identical with those applied in the investigation of CoO [2]. Therefore, only the details which are specific to NiO are presented.

EXPERIMENTAL PROCEDURES

A single crystal of NiO of full stoichiometry was kindly provided by the Laboratoire de Chimie des Solides, Université d'Orsay, France. It was synthesized by float-zone refining techniques from high-purity powder 5N. The crystal was cleaved several times parallel to the (001) crystal faces. It was hard and, when sufficiently thin, optically fully transparent with a glittering emerald green color. The surface of cleavage was seen to be perfectly smooth. The sample chosen for the X-ray diffraction measurements was a parallelepiped of size $0.140 \times 0.166 \times 0.191$ mm^3.

An accurate X-ray diffraction study was carried out for the antiferromagnetic phase at 298 K, which is well below the Néel temperature.

No antiferromagnetic distortion from the NaCl-type structure could be detected. So, the NiO crystal attained a face-centered cubic structure of the symmetry group $Fm\bar{3}m$. Least-squares refinement based on the X-ray diffraction pattern yielded a lattice constant of 4.169(2) Å.

Background, Lorentz, and polarization corrections were made for the intensities, as described by [4], as well as the absorption corrections of Busing and Levy [5] using a linear absorption factor of 25.266 mm^{-1}.

The TDS contaminations were evaluated with the program described in [6] using the elastic constants from [7]. These effects were small, less than 3% in intensity, owing to the hardness of the compound.

TREATMENT OF DATA

The data were submitted to the "direct multipole analysis" as described in the papers I and II on MnO and CoO, respectively. All that is said about the analysis in the context of the reference model and of the representation of results holds, even in detail, except for data referring specifically to the Ni atom and to the numerical values used or obtained, and will not be repeated here.

Table 1. Structure factors for NiO at 298 K

hkl	$2\sin\theta/\lambda$, Å^{-1}	F_0	F_c	δF_0	*y*
000	0.0000		144.000		
111	0.4155	64.5542	64.0979	0.3000	0.814
200	0.4797	101.3563	101.7546	0.3600	0.671
220	0.6784	81.6294	81.0661	0.2800	0.846
311	0.7955	49.0912	48.8074	0.2000	0.947
222	0.8309	67.8186	67.9548	0.2200	0.894
400	0.9595	57.9203	58.7623	0.2800	0.948
331	1.0455	38.8308	37.8826	0.1600	0.975
420	1.0727	51.7354	51.9476	0.1800	0.963
422	1.1751	47.0126	46.7107	0.0800	0.967
333	1.2474	31.2755	30.8269	0.1200	0.985
511	1.2464	30.0476	30.8269	0.1000	0.988
440	1.3569	38.7198	39.2371	0.1500	0.985
531	1.4191	25.5984	26.1219	0.1000	0.992
442	1.4391	35.7992	36.4847	0.1600	0.984
600	1.4391	37.2116	36.4847	0.1500	0.981
620	1.5170	34.1881	34.1735	0.1200	0.986
533	1.5729	22.4179	22.8432	0.0800	0.994
622	1.5911	31.6273	32.1993	0.1300	0.988
444	1.6618	31.0151	30.4865	0.1600	0.987
551	1.7130	20.1959	20.4434	0.0800	0.996
711	1.7130	20.8307	20.4434	0.0800	0.995
640	1.7297	29.1224	28.9795	0.1000	0.992
642	1.7950	27.5818	27.6368	0.1100	0.993
553	1.8424	18.9250	18.5985	0.0800	0.996
731	1.8424	18.8033	18.5985	0.0800	0.996
800	1.9189	25.4622	25.3260	0.1100	0.994

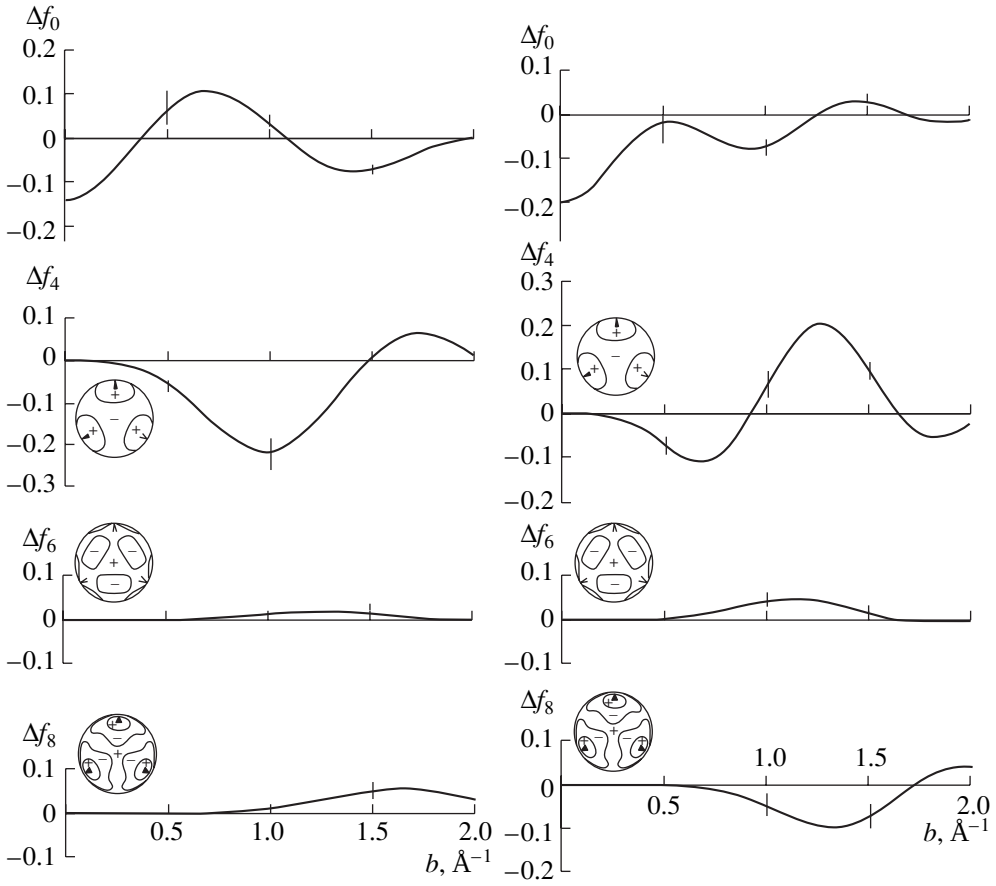

Fig. 2. Radial multipolar scattering factors of the ions in the antiferromagnetic state of NiO at 298 K for Ni^{2+} and O^{2-} within the partitioning radii R_{Ni} = 1.05 Å and R_O = 1.30 Å. The results refer to cubic harmonics normalized to the maximum value $K_n(\theta, \varphi)$ = 1, and the curves represent deviations Δf_n from the reference model.

For the Ni^{2+} ion of the reference model, the relativistic Hartree–Fock values of the International Tables for Crystallography [8] were used with the anomalous scattering factors f' = 0.285 and f'' = 1.113 from [9] for MoK_α.

Table 2. Spherical characteristics of the ionic electron distributions: radius r_0 of best separation at which the radial accumulation-of-charge density $s_0(r)$ reaches its minimum; the minimum radial density $s_{0\,min} = s_0(r_0)$; the electron count $Z_0 = Z_0(r_0)$ within the radius of best separation; and the radii r_{2+} and r_{2-}, where the electron counts reach the values 26 e and 10 e corresponding to the doubly ionized states

Ni^{2+}	r_0, Å	s_{0min}, e/Å	Z_0, e	r_{2+}, Å
Experimental 298 K	0.95	3.317	25.64	1.07
Reference model 298 K	1.05	4.031	26.09	1.03
O^{2-}	r_0, Å	s_{0min}, e/Å	Z_0, e	r_{2-}, Å
Experimental 298 K	1.20	2.775	8.97	1.43
Reference model 298 K	1.15	4.766	8.74	1.37

For NiO, the isotropic mosaic-spread extinction gave a lower R factor, 0.006, than the particle-size extinction, 0.007, and yielded the value $g = 0.040(2) \times 10^4$ rad^{-1} for the mosaic spread parameter and values B_{Ni} = 0.316 (0.016) Å^2 and B_O = 0.426 (0.047) Å^2 for the isotropic Debye–Waller factors. No additional significant improvement was obtained by any of the more sophisticated models.

In the successive iterative local Fourier-refinement of the scale and Debye–Waller factors, the scale factors remained unchanged, while B_{Ni} = 0.313 Å^2 and B_O = 0.420 Å^2 were obtained as the final refined values of the Debye–Waller factors of the reference model.

The results are represented by figures and tables in correspondence with the studies on MnO and CoO.

Colored versions of Fig. 5 are available at the Internet address http://bus.cines.fr/vidaljp/mag3D.

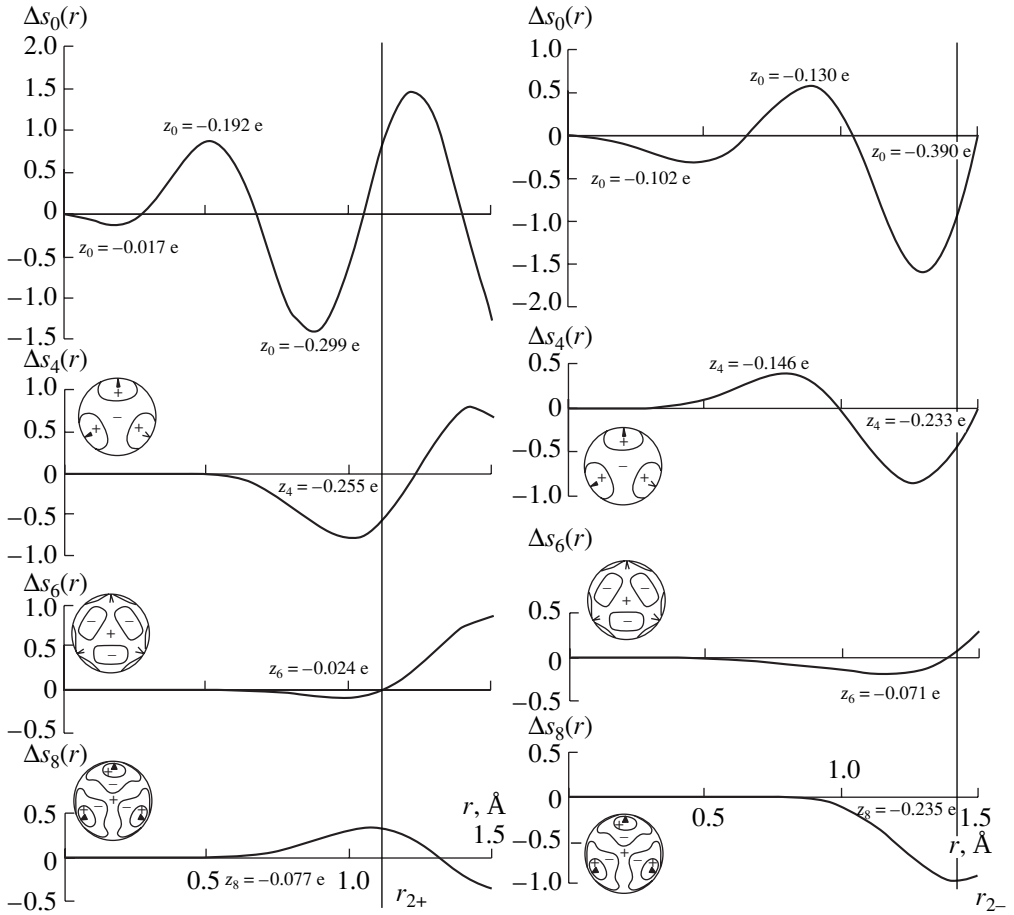

Fig. 3. Multipolar accumulation-of-charge densities $s_n(r)$ around the ionic sites in the antiferromagnetic state of NiO at 298 K for Ni^{2+} and O^{2-}. The curves represent deviations Δs_n from the reference model.

DISCUSSION

The radial density $s_0(r)$ of the oxygen in Fig. 1 has a clear resemblance to the oxygen in CoO. There is a "bump" similar to the intermediate maximum observed in CoO with a corresponding reduction of density at lower *r*. In NiO, this feature, however, clearly belongs to the main peak of oxygen and does not cause any ambiguity of the radius of best separation. According to the minimum value of $s_0(r)$, the separation of the oxygen from its surroundings is as good as in the paramagnetic MnO. The electron count of the oxygen peak is now the "normal" 9 e as in MnO, in accordance with the earlier observations on oxide peaks [10, 11].

The separating minimum of the cation is deeper and sharper than in the reference model, as in CoO and in the antiferromagnetic MnO. The shape of the minimum is even sharper and leads to a well-defined radius of best separation, although the minimum density $s_0(r_0)$ in NiO is essentially larger than in the antiferromagnetic CoO and about the same as in the antiferromagnetic MnO. The electron count of the peak is close to 26 e and corresponds to the doubly ionized state Ni^{2+}. The value $s_0(r_0)$ is, however, remarkably higher than one would expect for an ion [4, 10].

The density maps in Fig. 4 form the final tool of the analysis. In the map representations, the only significant features are those which are significant in the angular-integral representation in Fig. 3. Thus, no notice needs to be paid to the different densities at the ionic centers in any of the maps. Similarly, any local features of the Fourier maps that do not appear in the multipolar maps in Fig. 4 do not arise from the integral systematics of the low-order multipoles and must be regarded insignificant. Comparison with the multipolar maps makes it possible to determine how features in the Fourier maps originate from the different atoms [12].

Features denoted by *A*, *B*, and *C* in the maps and in Fig. 5 deserve to be discussed. These notations indicate correspondences with features of the CoO density maps, which are labeled similarly.

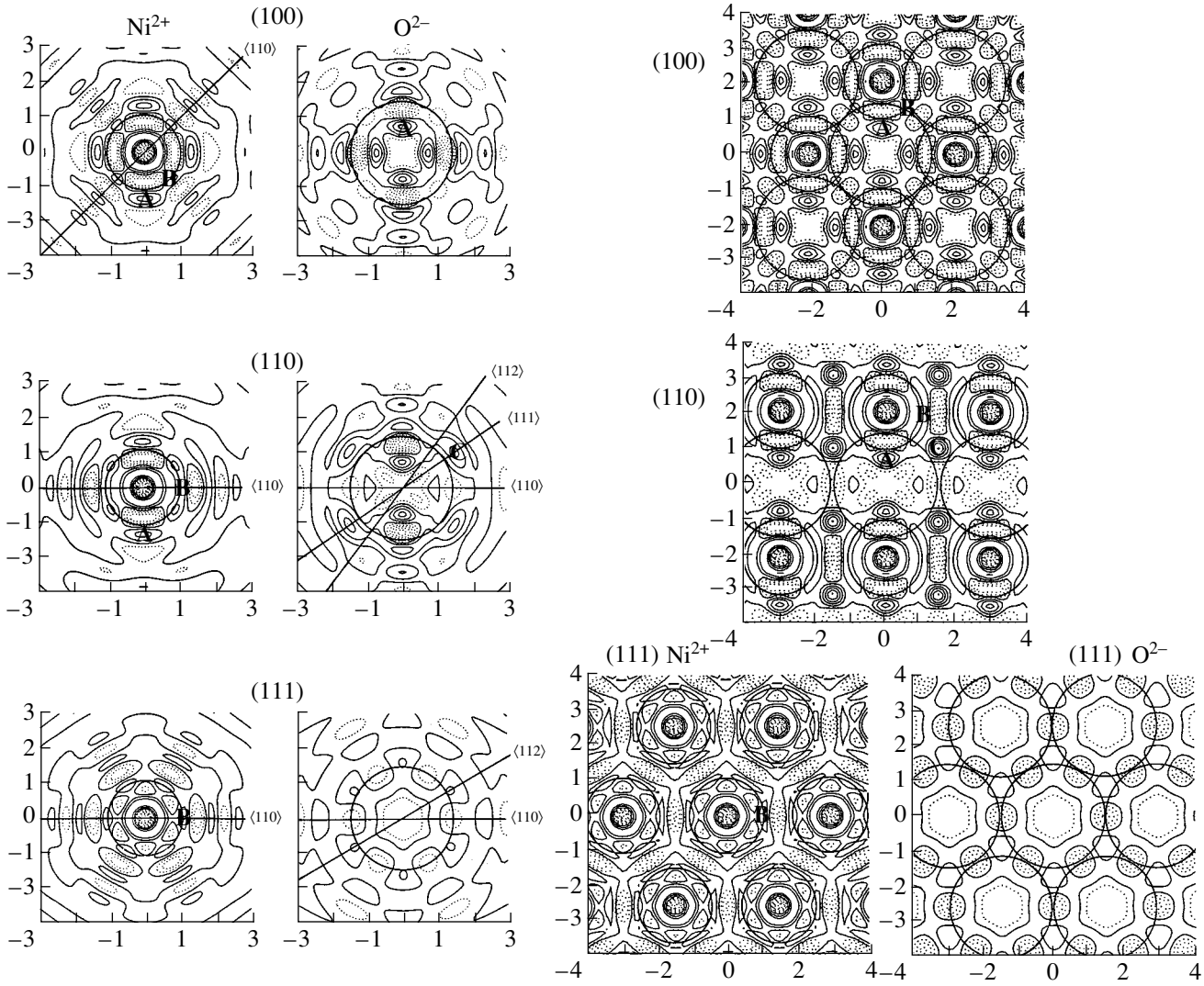

Fig. 4. Difference density maps of the multipole expansions up to $n = 8$, together with the corresponding Fourier difference-density maps on the lattice planes (100), (110), and (111), that pass through the ionic sites in the antiferromagnetic state of NiO at 298 K. The circles indicate the radii of doubly ionized ions. Solid lines indicate positive values; dashed lines, negative values; and dotted lines, zero values.

Feature A, with density maxima between the nearest neighbors O⟨100⟩Ni, looks much like covalent metal–oxygen bonding as in CoO. It is well within the oxygen area, unlike in CoO, where it is in the cation region. Still, we note from the multipolar maps that, as in the antiferromagnetic CoO, these maxima belong to the three-dimensional integral behavior of both ions. It should, thus, be interpreted as a result of an O⟨100⟩Ni coupling; this may be an indication of a superexchange effect.

The "bump" in the radial density $s_0(r)$ of oxygen in Fig. 1 has, thus, a different origin than the similar-looking intermediate maxima in CoO. This is caused by "bonding feature" A, whereas in CoO the maxima were related to the electronic-cage formation around the oxygen by the "B feature" that also caused the localization of the outer electrons of the O^{2-} ions.

Additionally, an electronic-cage structure appears here that is formed by the B-feature. While each oxygen atom had an octahedral cage of its own in the paramagnetic CoO, there is a cubic cage surrounding each Ni atom of the antiferromagnetic NiO, as shown in Fig. 5. According to the multipolar maps, this is strictly a feature of Ni without any significant coupling to the other features.

Feature C is visible in the (110) Fourier map as strong local maxima between the O⟨111⟩Ni neighbors. In the multipolar maps, it is present in the (110) oxygen map, but only as a much weaker effect. Therefore, it is strictly a feature of oxygen with somewhat questionable significance, like the corresponding features in

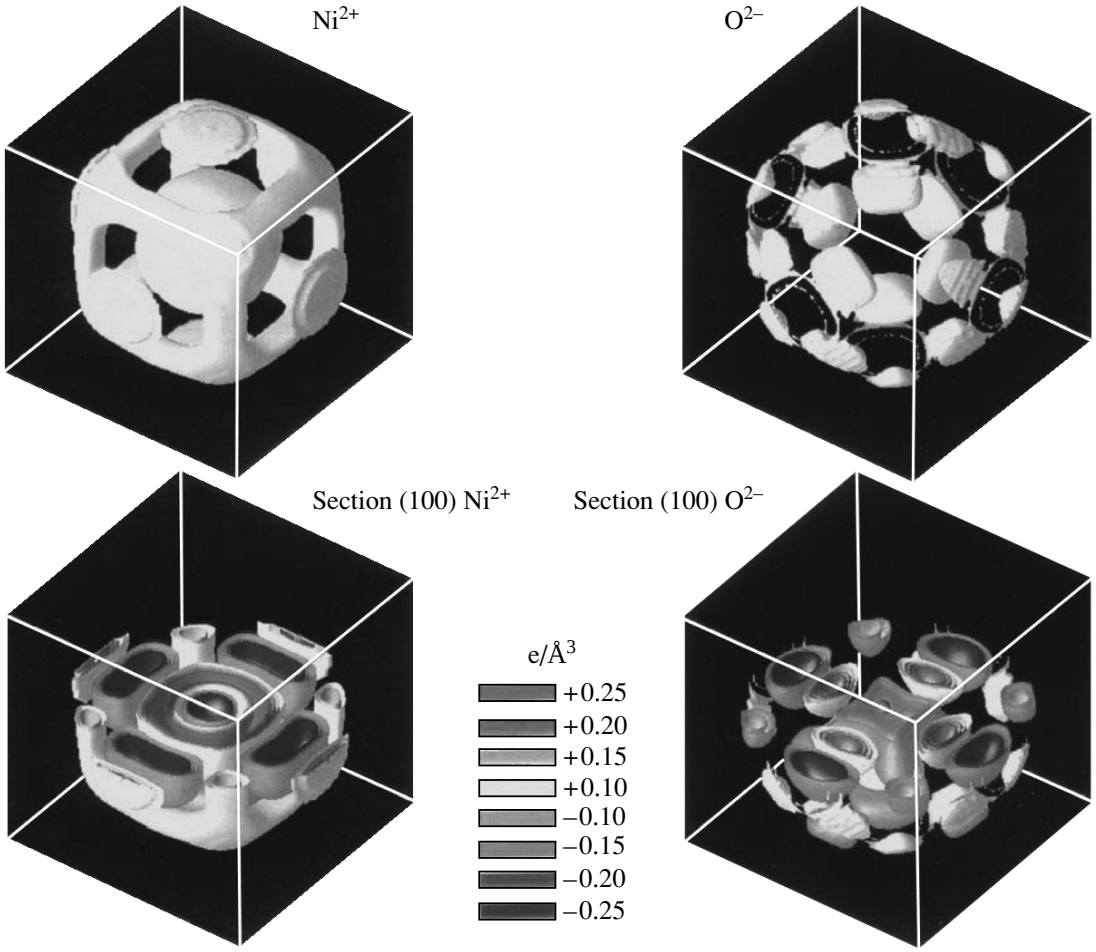

Fig. 5. Three-dimensional view on the equivalue surfaces of the ionic multipole expansions in the antiferromagnetic state of NiO at 298 K. For the color version of this figure, see http://bus.cines.fr/vidaljp/mag3D.

MnO, while in CoO it was interpreted to be an indication of electronic O⟨111⟩Co coupling. The C-maxima are also well separated from the other features both in the Fourier maps and in the multipolar maps. There is, thus, no clear indication of an extended network buildup, which is contrary to CoO, where the net buildup was quite strong, particularly in the antiferromagnetic state.

The problem of estimating the significance of such features in real space as revealed by the present method of analysis, in comparison with the accuracies obtained for the model parameters in the traditional fitting methods, has been discussed by [12]. While the significance or insignificance is merely due to the accuracy of measured data, it is expressed only by the errors bars in $\Delta f_n(b)$, reflecting the large-scale integral nature of the information, and cannot be transformed into local accuracy statements. Local features can be regarded significant to the relative extent expressed by the error bars as far as they are parts of the integral multipolar behavior.

ACKNOWLEDGMENTS

We thank the CINES, Centre Informatique National de l'Enseignement Supérieur (Montpellier, France), for financial support and technical assistance.

REFERENCES

1. J.-P. Vidal, G. Vidal-Valat, K. Kurki-Suonio, and R. Kurki-Suonio, Kristallografiya **47** (3), 391 (2002) [Crystallogr. Rep. **47**, 347 (2002)].
2. J.-P. Vidal, G. Vidal-Valat, K. Kurki-Suonio, and R. Kurki-Suonio, Kristallografiya **49** (3), 422 (2004) [Crystallogr. Rep. **49**, 357 (2004)].
3. R. Dovesi, R. Orlando, C. Roetti, *et al.*, Phys. Status Solidi B **217**, 63 (2000).

4. J.-P. Vidal, G. Vidal-Valat, M. Galtier, and K. Kurki-Suonio, Acta Crystallogr., Sect. A: Cryst. Phys., Diffr., Theor. Gen. Crystallogr. **37**, 826 (1981).
5. W. R. Busing and H. A. Levy, Acta Crystallogr. **10**, 180 (1957).
6. M. Merisalo and J. Kurittu, J. Appl. Crystallogr. **1**, 179 (1978).
7. K. G. Subhadra and D. B. Sirdeshmukh, Indian J. Pure Appl. Phys. **16**, 693 (1978).
8. *International Tables for X-ray Crystallography* (Kluwer Academic, Dordrecht, 1999), Vol. C.
9. D. T. Cromer and D. Liberman, J. Chem. Phys. **53**, 1891 (1970).
10. G. Vidal-Valat, J.-P. Vidal, and K. Kurki-Suonio, Acta Crystallogr., Sect. A: Cryst. Phys., Diffr., Theor. Gen. Crystallogr. **34**, 594 (1978).
11. G. Vadal-Valat, J.-P. Vidal, K. Kurki-Suonio, and R. Kurki-Suonio, Acta Crystallogr., Sect. A: Cryst. Phys., Diffr., Theor. Gen. Crystallogr. **43**, 540 (1987).
12. K. Kurki-Suonio, in *Proceedings of Symposium Franco–Finlandais: Structure de la Matiere, Repartitions Electroniques dans les Cristaux, Paris, 1993*, Ed. by J.-P. Vidal (Montpellier, 1994), p. F1; in *Structural Studies of Crystals: Honour of the 75th Anniversary of Academician Boris Vaĭnshteĭn*, Ed. by V. Simonov (Nauka, Moscow, 1996), pp. 46–64 [in Russian].